ACS APPLIED ELECTRONIC MATERIALS

pubs.acs.org/acsaelm

Article

Optical Properties of Superconducting $Nd_{0.8}Sr_{0.2}NiO_2$ Nickelate

Rebecca Cervasio, Luca Tomarchio, Marine Verseils, Jean-Blaise Brubach, Salvatore Macis, Shengwei Zeng, Ariando Ariando, Pascale Roy,* and Stefano Lupi*

Cite This: ACS Appl. Electron. Mater. 2023, 5, 4770−4777

Read Online

ACCESS | Metrics & More | Article Recommendations | Supporting Information

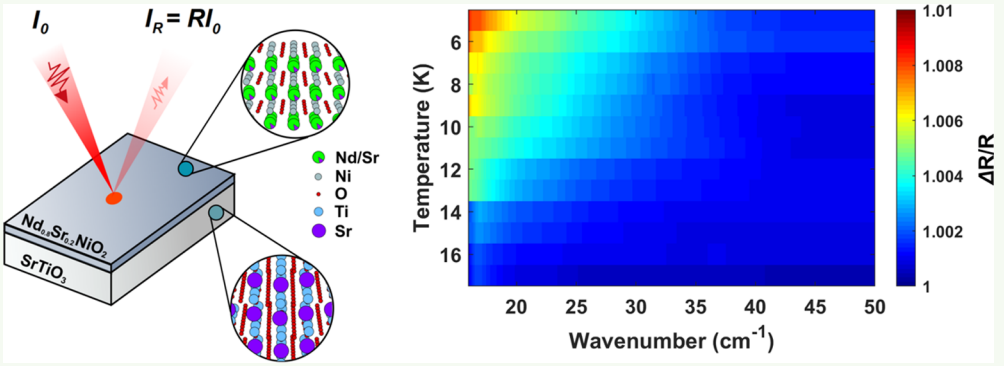

ABSTRACT: The intensive search for alternative noncuprate high-transition-temperature (T_c) superconductors has taken a positive turn recently with the discovery of superconductivity in infinite-layer nickelates. This discovery is expected to be the basis for disentangling the puzzle behind the physics of high T_c values in oxides. In the unsolved quest for the physical conditions necessary for inducing superconductivity, we report on a broad-band optical study of a $Nd_{0.8}Sr_{0.2}NiO_2$ film measured using optical and terahertz spectroscopy at temperatures above and below the critical temperature $T_c \sim 13$ K. The normal-state electrodynamics of $Nd_{0.8}Sr_{0.2}NiO_2$ can be described by a scattering time at room temperature ($\tau \simeq 1.3 \times 10^{-14}$ s) and a plasma frequency $\omega_p \simeq 5500$ cm^{-1} in combination with an absorption band in the mid-infrared (MIR), characteristics of transition metal oxides, located around $\omega_0 \sim 2500$ cm^{-1} and with an amplitude ω_p^{MIR} of about 8000 cm^{-1}. The degree of electronic correlation can be estimated using the ratio $\omega_p^2/(\omega_p^2 + (\omega_p^{MIR})^2)$. In the present system, the determined value of 0.32 ± 0.06 indicates a strong electron correlation in the NiO_2 plane with similar strength as cuprates. From 300 to 20 K, we observe a spectral weight transfer between the Drude and MIR band, together with a strong increase in the Drude scattering time, in agreement with DC resistivity measurements. Below T_c, a superconducting energy gap $2\Delta \sim 3.3$ meV can be extracted from the terahertz reflectivity using the Mattis−Bardeen model.

KEYWORDS: *unconventional superconductivity, nickelates, superconducting gap, THz spectroscopy, optical spectroscopy, electrodynamics of superconductors*

INTRODUCTION

The complex physics behind the superconductive phase in high-temperature superconductors like cuprates still holds unknown facets nearly 35 years after their first discovery by Bednorz and Mueller.[1] In particular, the search for the pairing mechanism in cuprates has been a major research focus. To explore this mechanism, additional high-T_c superconductors families were explored, with different transition metals but similar crystal and electronic structures.[2,3] One such family, the nickelates, is built from two-dimensional (2D) planes of NiO_2 interchanged with dopant ions that form spacer layers, equivalent to the CuO_2 planes in cuprates. A superconductive phase was recently verified experimentally in Sr-doped $NdNiO_2$ thin films grown on STO substrates, more than 20 years after their first theoretical prediction.[4]

The infinite-layer nickelate, $Nd_{0.8}Sr_{0.2}NiO_2$ (NdSrNiO), is synthesized via soft chemistry topotactic reduction[5] on an STO substrate reaching a type-II superconductive phase with a relatively high transition temperature of about 9−15 K.[6] The presence of the substrate is essential for producing the superconductive phase, giving an unusual picture in which the substrate both strains the crystal and stabilizes this phase. As for other unconventional superconductors, the superconductivity is induced by charge doping in the parent compound. Although the phase diagram of $Nd_{1-x}Sr_xNiO_2$ shows a superconductive dome, with the highest critical temperature (of about 15 K) at Sr doping $x = 0.2$,[7] nickelates

Received: April 18, 2023
Accepted: August 1, 2023
Published: August 16, 2023

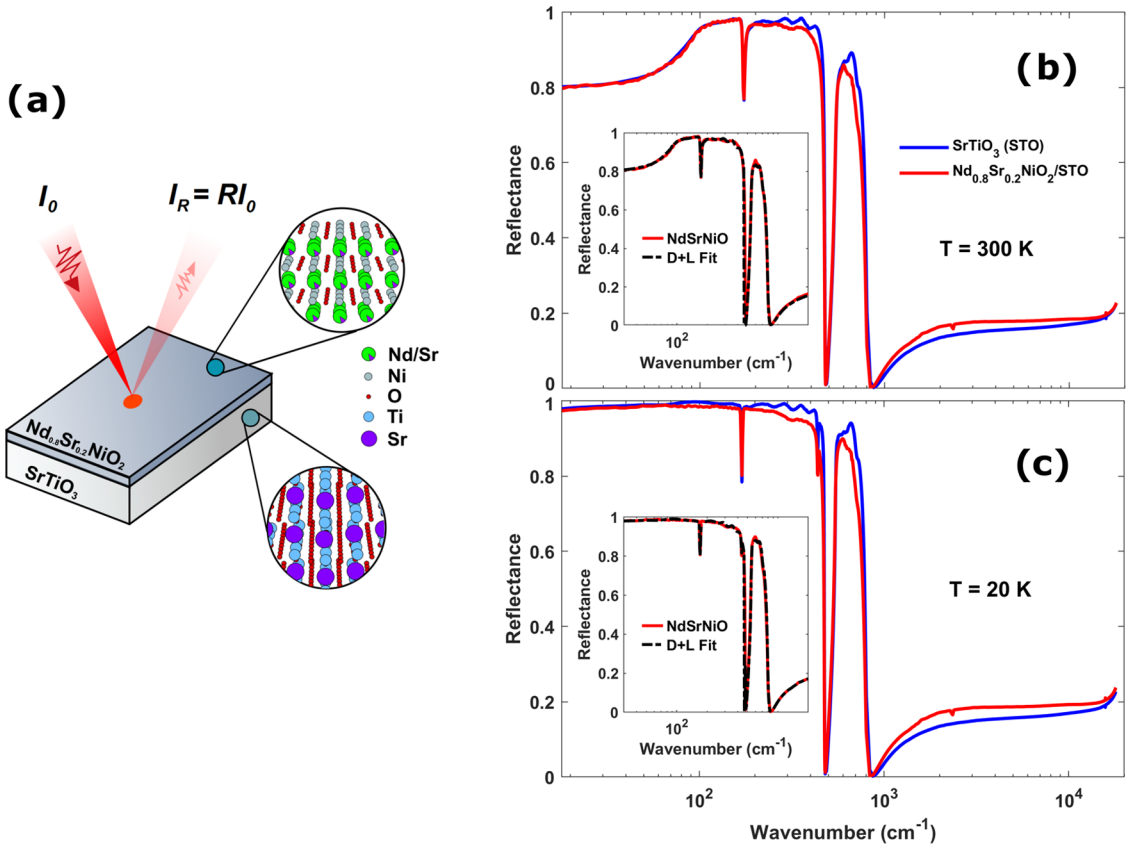

Figure 1. Reflectance spectroscopy of a $Nd_{0.8}Sr_{0.2}NiO_2$/STO thin film. (a) Schematic view of $Nd_{0.8}Sr_{0.2}NiO_2$/STO thin-film sample and incoming I_0 and reflected light intensity $I_R = RI_0$ (R is the reflectance). Crystal structures are represented in the magnification circles. (b, c) Broad-band reflectance spectra of $Nd_{0.8}Sr_{0.2}NiO_2$/STO thin film (red line) and STO substrate (blue line) at 300 (b) and 20 K (c), respectively. The insets show the Drude−Lorentz (D + L) best fit of NdSrNiO/STO as obtained using an air/film/STO trilayer model (see Figure S3 in the SI for details) and a Drude−Lorentz conductivity (eq 1) for the film.

reveal many differences with respect to cuprates. The most noticeable distinction is that no evidence of magnetic ordering is experimentally observed.[5−7] Moreover, Hall measurements[6] and ab initio simulations[8−12] highlighted a complex picture behind the symmetry of the order parameter, in which the superconductive mechanism appears inconsistent with the picture of a simple hole-doped electronic band. Indeed, the description of the electronic structure near the Fermi level might require up to three bands and their hybridization,[13] and contributions coming from the 4*f* shells have also been proposed.[14] Furthermore, the role of electronic correlations has been pointed out recently,[15] although an experimental estimate of their importance is still lacking. On the other hand, the electron−phonon coupling has been ruled out as the exclusive origin of the observed superconductivity,[13] with spin fluctuations playing a key role despite the absence of long-range magnetic order.[12,16]

To determine the superconducting gap (2Δ) and the pairing mechanism of the superconducting state, terahertz (THz) and microwave absorption spectroscopy,[17−19] tunneling spectroscopy,[20] specific heat,[21,22] and London penetration depth techniques are the prevailing experimental methods. In the case of $Nd_{1-x}Sr_xNiO_2$, London penetration depth measurements produce consistent data between different independent reports.[23,24] Still, the paramagnetic background and limited quality of the samples leave the interpretation open to further debate. Moreover, tunneling measurements on $Nd_{1-x}Sr_xNiO_2$ were also performed,[25] suggesting the presence of two different superconducting gaps at 3.9 and 2.35 meV.

On the other hand, no optical investigations of $Nd_{0.8}Sr_{0.2}NiO_2$ films have been reported, at least to our knowledge, either in the normal or in the superconducting state. This is mainly due to the presence of the $SrTiO_3$ substrate, reflecting close to 100% of the THz light through its soft phonon mode. Since optical investigations contributed a great deal to shed light on high-temperature superconductivity mechanisms through evaluations of the superconductive gap, the scattering mechanism, and coherence effects,[26−32] these measurements are highly longed for.

In the present study, we report on the optical reflectance $R(\omega)$ of a high-quality optimally doped $Nd_{0.8}Sr_{0.2}NiO_2$ film over an STO substrate across a broad range of frequencies ω, from terahertz (15 cm^{-1}) to visible (VIS, 20,000 cm^{-1}), as obtained by combining THz radiation, generated from the AILES beamline@Soleil third-generation synchrotron machine, with conventional optical spectroscopy. The normal-state optical conductivity, $\sigma(\omega)$, derived from these measurements, provides the first experimental indication of strong electronic correlation in the NiO_2 plane. Indeed, $\sigma(\omega)$ is described by a superposition of a Drude term (representing the coherent motion of charge carriers in the NiO_2 plane) and an absorption band in the mid-IR (representing their incoherent motion and generated by strong correlations). This scenario is common to other metallic oxides, including cuprates, and suggests an important role of electronic correlations in the

https://doi.org/10.1021/acsaelm.3c00506
ACS Appl. Electron. Mater. 2023, 5, 4770−4777

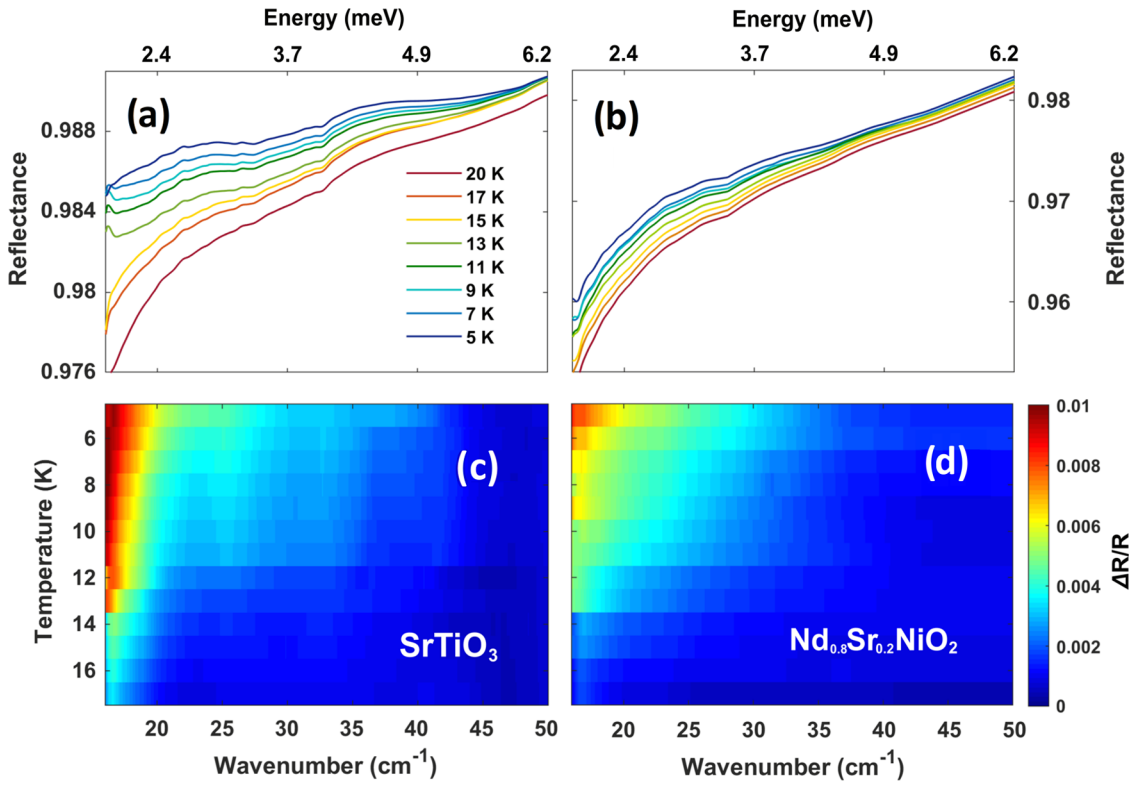

Figure 2. Temperature-dependent analysis of a $Nd_{0.8}Sr_{0.2}NiO_2$/STO THz reflectivity. (a) Absolute THz reflectance of the STO substrate at different temperatures. (b) THz reflectance of the $Nd_{0.8}Sr_{0.2}NiO_2$ film over the STO substrate at different temperatures. At frequencies (ω > 50 cm^{-1}), the curves merge toward a common absolute value. (c, d) Contour plots of the relative THz reflectance for both the sample and bare substrate, as a function of temperature (5−20 K) and frequency. Relative spectra were calculated by dividing the measurements by equivalent measurements at 20 K.

NiO_2 plane. Finally, in the superconducting state, an energy gap ($2\Delta \sim 3.3$ meV) is evaluated by fitting the THz reflectance at different temperatures with a Mattis−Bardeen model.

EXPERIMENTAL RESULTS

All reflectance measurements were performed on a 10 nm thick, optimally doped $Nd_{0.8}Sr_{0.2}NiO_2$ film, grown on a 500 μm $SrTiO_3$ (STO) (001) substrate through soft chemistry topotactic reduction using CaH_2 (see the Methodssection). The optical properties of the actual STO substrate were measured in the same experimental conditions. The infinite-layer structure of $Nd_{0.8}Sr_{0.2}NiO_2$ and the perovskite structure of STO are represented in Figure 1a. Prior to optical measurements, superconductivity was verified by resistance measurements as a function of temperature, showing $T_c \simeq 13$ K (see Figure S1 in the Supporting Information (SI)).

The optical reflectance measured at 300 K is shown in Figure 1b, across a wide range of frequencies, from THz to VIS for both the $Nd_{0.8}Sr_{0.2}NiO_2$ film and STO substrate. A gold layer evaporated on both film and substrate has been used as a reference for reflectance absolute measurements. For the STO substrate, a series of strong transverse optical (TO) phonon modes are observed. Starting from lower frequencies, these can be identified as[33,34] TO_1 at 100 cm^{-1} (soft mode), TO_2 at 176 cm^{-1}, and TO_3 at 540 cm^{-1}. The reflectance of the $Nd_{0.8}Sr_{0.2}NiO_2$ film shows similar behavior to STO with a small decrease above 200 cm^{-1}, mainly related to the Drude metallic absorption, and an increase above 1000 cm^{-1} associated with the (MIR absorption band (see the discussion of eq 1)).

THz reflectance measurements of film and substrate were also performed as a function of temperature between 5 and 20 K in the frequency range of 15−50 cm^{-1} (all curves at different T's merge above this frequency), crossing the film superconductive critical temperature at $T_c \sim 13$ K. Figure 2a shows the STO reflectance at these temperatures and frequency ranges in a very expanded vertical scale. The increase in the substrate reflectance at low frequencies is due to the STO soft mode. This well-known effect is further highlighted in Figure S2 in the SI. In contrast, $R(\omega)$ of the film in the same temperature and frequency range (Figure 2b) shows a different relative change, suggesting a further effect induced by the superconducting transition.

To magnify these differences, we calculate the relative reflectance spectra $\Delta R/R = (I_R(T) - I_R(20\text{ K}))/I_R(20\text{ K})$ as obtained by dividing the light intensity reflected by the film or STO ($I_R(T)$) at all temperatures by the signal ($I_R(20\text{ K})$) at the reference temperature T = 20 K (>T_c). The results are shown in a 2D intensity plot for STO and $Nd_{0.8}Sr_{0.2}NiO_2$ film (Figure 2c,d, respectively) as a function of both temperature and frequency (the same results are shown as three-dimensional (3D) plots in Figure S4 in the SI). The 2D plots clearly highlight the differences between the bare substrate and the film THz properties *vs* T, supporting a different origin for the modification of the reflectance spectra at the lowest temperatures.

DISCUSSION OF RESULTS

Normal-State Optical Conductivity. To analyze the behavior of the $Nd_{0.8}Sr_{0.2}NiO_2$ film, it is necessary to consider the optical response of the substrate. To do so, the substrate optical data was analyzed through a Kramers−Kronig constrained fitting to extract the optical refraction index at every temperature[35] (a fitting example for STO is shown in the inset of Figure 1b). Therefore, the $Nd_{0.8}Sr_{0.2}NiO_2$ film is modeled in terms of an air/film/STO trilayer[36,37] and fitted through the RefFit program[35] (more information can be found in the Multilayer Stacking Model section and Figure 3 in the SI). The optical properties of $Nd_{0.8}Sr_{0.2}NiO_2$ in the normal state are well described in terms of a Drude−Lorentz model. The complex conductivity expressed in units of $S{\cdot}cm^{-1}$ takes the form[38]

https://doi.org/10.1021/acsaelm.3c00506
ACS Appl. Electron. Mater. 2023, 5, 4770−4777

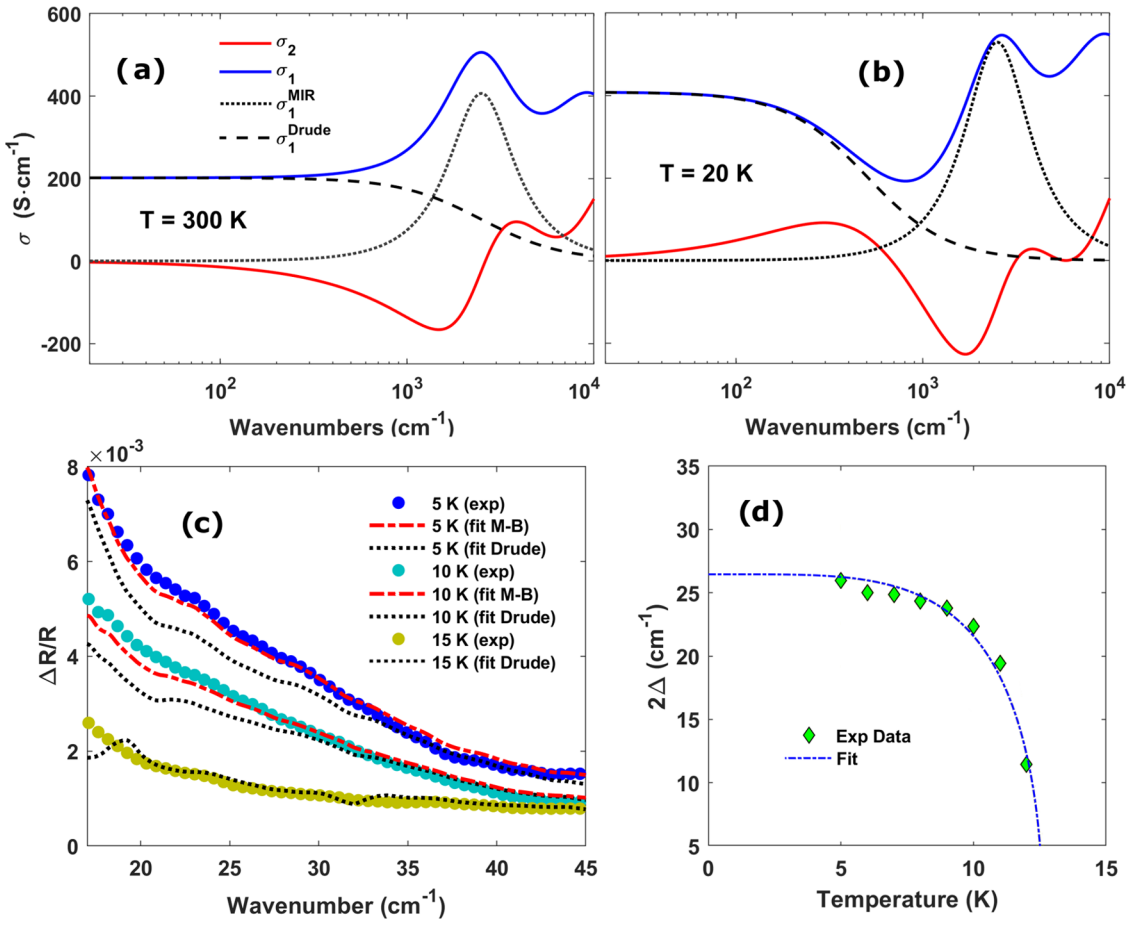

Figure 3. Optical conductivity and superconducting gap of $Nd_{0.8}Sr_{0.2}NiO_2$ superconductive film. (a, b) Real and imaginary parts of the optical conductivity of the $Nd_{0.8}Sr_{0.2}NiO_2$ superconductive film at 300 K (a) and 20 K (b), as extracted through a Drude−Lorentz fitting model (eq 1). Dashed and dotted lines show the real parts of the Drude and MIR oscillators, respectively. (c) Comparison between experimental relative reflectance (solid circles) at 5, 10, and 15 K with the relative reflectance deduced from the Mattis−Bardeen model (M−B, red, discontinuous lines) and the Drude model (black, dotted lines). This calculation was performed by taking the Drude term at 20 K and including the STO indices at 5, 10, and 15 K. (d) Superconducting gap values (green diamonds) as a function of temperature as determined by the M−B model at finite T (see text). The experimental data can be described in eq 5. The gap extrapolation to 0 K gives $2\Delta \simeq 26.5$ cm^{-1} (~3.3 meV) in good agreement with the literature.

$$\sigma(\omega) = \frac{2\pi}{Z_0}\frac{\omega_p^2}{\Gamma - i\omega} + \frac{2\pi}{Z_0}\sum_j \frac{\omega\omega_{p_j}^2}{\gamma_j\omega - i(\omega_{0_j}^2 - \omega^2)} \quad (1)$$

where Z_0 is the free space impedance (377 Ω) and the frequencies are expressed in units of cm^{-1}. In the Drude term, ω_p is the Drude plasma frequency, while $\Gamma = 1/\tau$ is the scattering rate, with τ being the scattering time. The Lorentz oscillators are instead described by their characteristic frequency (ω_{0_j}), intensity ($\omega_{p_j}^2$), and scattering rate (γ_j). The use of the model in eq 1 is supported by a vast literature concerning the optical conductivity of cuprates.[27] There, the description of the optical conductivity strongly depends on temperature, doping, and the type of cuprate family.[39−42] In such a complex framework, the fitting of the conductivity, in particular, for thin films, should minimize the number of absorption terms to be used in eq 1. Here, a model based on a Drude term plus two Lorentz oscillators located in the mid-IR and near-IR (NIR) is sufficient to fit the reflectance curve for $Nd_{0.8}Sr_{0.2}NiO_2$ from THz (15 cm^{-1}) to the visible spectrum (20,000 cm^{-1}) (see the inset of Figure 1b,c). In the fitting procedure, the real (n) and imaginary (k) parts of the STO refraction index have been used as inputs, taking into account the contribution to the whole (film+substrate) reflectance coming from this substrate layer. The STO substrate optical characterization, in agreement with the literature,[33,34] is available in the SI (Figure 2).

Figure 3a,b shows the real ($\sigma_1(\omega)$, blue line) and imaginary parts ($\sigma_2(\omega)$, red line) of the resulting optical conductivity for the $Nd_{0.8}Sr_{0.2}NiO_2$ film in its normal state at 300 and 20 K, together with the Drude term (dashed line) and the MIR band (dotted line). The NIR band, appearing around 10,000 cm^{-1}, is probably reminiscent of the electronic gap in the insulating $NdNiO_2$ material. A Drude plasma frequency $\omega_p \sim 5500$ cm^{-1} is extracted from the fitting at 300 K, together with a scattering time $\tau \sim 1.3 \times 10^{-14}$ s. Such a low scattering time is probably related to the quasi-2D geometry of the material. The MIR band is centered at $\omega_0^{MIR} \sim 2500$ cm^{-1} with an amplitude of $\omega_p^{MIR} \sim 8000$ cm^{-1} (all fitting parameters are reported in Table S1 in the SI). The MIR band is a common feature of many transitional metal oxides including cuprate- and iron-based superconductors, being related to electronic correlations. These usually renormalize the Drude term (coherent charge excitations), transferring spectral weight to an incoherent one

https://doi.org/10.1021/acsaelm.3c00506
ACS Appl. Electron. Mater. 2023, 5, 4770−4777

at finite frequencies (MIR band).[43,44] In particular, the $\omega_p^2/(\omega_p^2 + (\omega_p^{MIR})^2)$ ratio provides an experimental estimate for the degree of electronic correlation of the material.[45] While for weakly correlated metals, such as gold and silver, one obtains $\omega_p^2/(\omega_p^2 + (\omega_p^{MIR})^2) \sim 1$, for $Nd_{0.8}Sr_{0.2}NiO_2$, this ratio reaches a value of about 0.32 ± 0.06 at 300 K. This value can be compared to those of other correlated oxides like V_2O_3 (~0.18) and cuprates (0.2−0.4),[46] identifying $Nd_{0.8}Sr_{0.2}NiO_2$ as a strongly correlated electronic system. This is an important result of our paper as it provides an experimental constraint for all theoretical models describing the low-energy electronic states of NiO_2.[15]

A similar fitting occurred at 20 K (see Table S1 in SI), highlighting a transfer of spectral weight from the Drude term to the MIR band, as further expected for correlated systems[44,45] (see Figure 3a,b). Moreover, the increase of the Drude scattering time from 300 K ($\tau \sim 1.3 \times 10^{-14}$ s) to 20 K ($\tau_{20K} \sim 6.7 \times 10^{-14}$ s) is in good agreement with the DC resistivity temperature behavior of similarly doped samples.[47] Through the scattering time value at 20 K, it is possible to estimate whether the $Nd_{0.8}Sr_{0.2}NiO_2$ nickelate is in the clean ($\hbar/\tau < 2\Delta$) or in the dirty ($\hbar/\tau > 2\Delta$) limit for superconductivity. As the superconductive gap energy 2Δ is measured at 3.9 meV by tunneling spectroscopy,[25] we can calculate the ratio $\hbar/2\Delta = 1.7 \times 10^{-13}$ s, and by comparing it with our scattering time τ, we obtain $\tau < \hbar/2\Delta$, suggesting that the material is in the dirty limit. The coherence of this result will be verified in the next section, where we estimate the superconducting gap from reflectance measurements below T_c.

The scattering time τ can also be related to the critical temperature T_c of the superconductor through the well-known relation $\hbar/\tau \approx 2k_BT_c$, which is valid for cuprate high-temperature superconductors, both in the bulk[38] and thin-film limit.[48] This relation finds its origin in the scaling factor for cuprates proposed by Homes et al.[49,50] and supported by Tallon et al.,[51] in which the normal-state conductivity is established to be proportional to the product of the superfluid density with T_c. The result for the nickelate film, however, departs from this relationship since $\hbar/\tau$ is higher than $2k_BT_c$: $\hbar/\tau \sim 9$ meV > 2.2 meV $\sim 2k_BT_c$.

In cuprates, the scaling factor $\hbar/\tau \approx 2k_BT_c$ has been suggested to result from either a marginal Fermi-liquid state, a Josephson coupling between planes, the scattering of impurities for a d-wave order parameter, or even a BCS dirty limit superconductivity.[51] In the present (nickelate) case, in which this scaling factor does not stand, the physical implications remain unclear but nevertheless add to the differences between the two families of superconducting oxides.

Optical Determination of the Superconducting Gap. In Figure 2b, we show the absolute reflectance of $Nd_{0.8}Sr_{0.2}NiO_2$ film onto STO at different temperatures in the superconducting state and in the normal state at 20 K. In Figure 2a, the same quantity is represented for the bare STO substrate. The two reflectances show different temperature dependence. For STO, this is due to the soft phonon mode, while for $Nd_{0.8}Sr_{0.2}NiO_2$ on STO reflectance, its temperature dependence is related to a combination between the superconductivity transition and the STO soft mode.

In order to extract the superconducting gap and its temperature dependence, we fit the film's relative reflectance $\Delta R/R = [R(T < T_c) - R(20\ K)]/R(20\ K)$ at various temperatures below T_c. In the dirty limit of the electron transport (see below), the fitting process can be worked out by using the Mattis−Bardeen theory for a s-wave superconductor.[52] The s-wave assumption is supported by both STS and DC experiments.[6,25,53,54] The choice of using the relative reflectance measurements for understanding the superconducting transition is mainly justified by the high substrate absolute reflectance. Indeed, relative measurements grant a higher sensitivity when comparing different temperatures, and the use of the Mattis−Bardeen theory for the study of superconductive materials is well documented.[55−57] The real $\sigma_1^{sc}(\omega)$ and imaginary $\sigma_2^{sc}(\omega)$ parts of the optical conductivity in the superconducting state, normalized to those of the normal state $\sigma_N(\omega)$, take the form[52,57]

$$\frac{\sigma_1^{sc}}{\sigma_N} = \frac{2}{\hbar\omega}\int_{\Delta}^{\infty} dE[f(E) - f(E+\hbar\omega)]\mathcal{E}(E,\hbar\omega,\Delta) - \frac{\Theta(\hbar\omega - \Delta)}{\hbar\omega}\int_{\Delta-\hbar\omega}^{-\Delta} dE[1 - 2f(E+\hbar\omega)]\mathcal{E}(E,\hbar\omega,\Delta) \quad (2)$$

$$\frac{\sigma_2^{sc}}{\sigma_N} = \int_{-\Delta,\Delta-\hbar\omega}^{\infty} dE[1 - 2f(E+\hbar\omega)]\mathcal{E}(E,\hbar\omega,\Delta) \quad (3)$$

where

$$\mathcal{E}(E,\hbar\omega,\Delta) = \frac{E(E+\hbar\omega) + \Delta^2}{\sqrt{E^2 - \Delta^2}\sqrt{(E+\hbar\omega)^2 - \Delta^2}} \quad (4)$$

$f(E)$ is the Fermi−Dirac distribution, Δ is the superconductive gap, and Θ is the Heaviside function. In the expression for σ_2^{sc}, the lower limit of integration is taken as the largest between the two values $-\Delta$ and $\Delta - \hbar\omega$. σ_N is mostly dominated by its real part at THz frequencies.

Figure 3c shows the best-fit results. In particular, the dashed-dotted colored lines represent the relative reflectances at 15, 10, and 5 K, calculated by using the Mattis−Bardeen model for the film and the STO indices at each temperature for the substrate. The black dotted lines are instead reproduced through a Drude model for the film. The Drude coefficients at 20 K have been used in this calculation together with STO optical indices at 5, 10, and 15 K. Indeed, from the resistance curve (see Figure S1 in the SI), we do not expect a temperature variation of the Drude parameters below 20 K. As evident from Figure 3c, the Mattis−Bardeen model better describes $\Delta R/R$ in the superconducting state also providing the value of the superconducting gap 2Δ at different $T < T_c$. The superconducting gap behavior *vs* T is shown in Figure 3d. The gap opens near 13 K, in agreement with the resistance measurements and previous studies,[6,7] and rapidly increases for reducing T. To extrapolate 2Δ at 0 K, we fit its T dependence through the following equation[30,58]

$$2\Delta(T) = 2\Delta(0)\tanh\left(k\sqrt{\frac{T_c}{T} - 1}\right) \quad (5)$$

where the coefficient k accounts for the coupling symmetry, T_c is the critical temperature, and $2\Delta(0)$ is the superconducting gap at 0 K. The resulting fit is shown as a discontinuous blue line in Figure 3d. The extracted temperature $T_c \simeq 12.6 \pm 0.4\ K$ agrees with the DC resistance data in Figure 1 in the SI. The superconductive gap extracted at 0 K, $2\Delta(0) = 26.5 \pm 0.8$ cm^{-1}, agrees with the results obtained from tunneling measurements.[25] Although the parameter $k = 2.2 \pm 0.5$ is in

https://doi.org/10.1021/acsaelm.3c00506
ACS Appl. Electron. Mater. 2023, 5, 4770−4777

agreement with a s-wave coupling symmetry ($k = 2.2$),[59] due to the strong contribution of the substrate to reflectance measurements, we cannot exclude the presence of a second gap or a different coupling symmetry.[23,24]

CONCLUSIONS

In this work, we investigated the low-energy electrodynamics of the novel nickelate $Nd_{0.8}Sr_{0.2}NiO_2$ superconducting thin film by using broad-band optical spectroscopy from terahertz to visible. The normal-state electrodynamics of $Nd_{0.8}Sr_{0.2}NiO_2$ can be described at all temperatures above T_c by a Drude model characterized at 300 K by a scattering time of $\tau \sim 1.3 \times 10^{-14}$ s and a plasma frequency of $\omega_p \simeq 5500$ cm^{-1}, in combination with a mid-IR absorption band at about $\omega_0^{MIR} \sim 2500$ cm^{-1} with an amplitude of $\omega_p^{MIR} \sim 8000$ cm^{-1}. The $\omega_p^2/(\omega_p^2 + (\omega_p^{MIR})^2)$ ratio, like in cuprates and many transitional metal oxides, can be used to estimate the degree of electronic correlation in $Nd_{0.8}Sr_{0.2}NiO_2$.[45] This ratio is ~0.32 ± 0.06, setting the nickelate infinity layer family in a strong correlation level like many cuprates.[46] This is the most important result of this paper as it provides an experimental constraint for all theoretical models describing the low-energy electronic states of NiO_2.

Moreover, the scaling law ($\hbar/\tau \sim 2k_BT_c$) valid for high-T_c cuprates[38] is not satisfied by the $Nd_{0.8}Sr_{0.2}NiO_2$ superconductor ($\hbar/\tau \sim 9$ meV > 2.2 meV $\sim 2k_BT_c$). This indicates a further difference among charge fluctuations in the CuO_2 and NiO_2 planes. Finally below T_c, through the Mattis−Bardeen model, we estimate from the terahertz optical reflectance a superconducting gap close to 3.3 meV in good agreement with tunneling data.[25]

METHODS

Sample Preparation. We prepared and characterized our $Nd_{0.8}Sr_{0.2}NiO3$ thin-film samples following procedures previously described by Zeng et al.[7] The perovskite $Nd_{0.8}Sr_{0.2}NiO3$ thin films with a thickness of 10 nm were grown on a single polished TiO_2-terminated (001) $SrTiO_3$ (STO) substrate by using a pulsed laser deposition (PLD) technique. The deposition temperature, oxygen partial pressure P_{O_2}, and laser energy density were set to be 600 °C, 150 mTorr, and 1.8 J/cm^2, respectively. The samples were annealed for 10 min at 600 °C and 150 mTorr after deposition and then cooled to room temperature at a rate of 8 °C/min. The infinite-layer structure was obtained through a soft chemistry topotactic reduction using CaH_2 as the reagent. During the reduction process, the perovskite films were embedded into CaH_2 powder, wrapped in aluminum foil, and then heated in a PLD vacuum chamber. The samples were heated to 340−360 °C at a rate of 25 °C/min, kept for 80 min, and then cooled down to room temperature at a rate of 25 °C/min. In order to obtain the reflectance spectra through THz measurement, half of the infinite-layer thin film was covered by a 50 nm Au layer, which was deposited by evaporation.

Spectroscopic Measurements. The film optical properties from THz to VIS were probed by using a combination of different spectrometers. The THz reflectance measurements have been performed at the infrared spectroscopy beamline AILES (Advanced Infrared Line Exploited for Spectroscopy), Synchrotron SOLEIL.[60] Exploiting the high brightness of the synchrotron radiation source, THz spectra in the 10−600 cm^{-1} range and MIR spectra (up to 6000 cm^{-1}) were obtained using a Bruker IFS125HR Fourier transform spectrometer evacuated at pressures lower than 10^{-4} mbar to avoid absorption by water and residual gas. The (10−60 cm^{-1}) spectral range was measured with a resolution of 0.5 cm^{-1} using a 50 μm Mylar beamsplitter combined with a bolometer cooled at 1.6 K, having a signal-to-noise ratio of 1700:1. The error bar on the measured reflectivity is 0.2%. For the (40−600 cm^{-1}) range, a spectral resolution of 2 cm^{-1} was obtained using a 6 μm Mylar combined with a bolometer cooled at 4.2 K. Above 600 cm^{-1}, an MCT detector cooled at 4.2 K was used, together with a KBr beamsplitter. A low-vibration pulse tube cryostat was used to achieve temperatures down to 5 K from room temperature. This system contains a sample holder which is mechanically decoupled from its coldfinger, allowing minimum sample vibrations. The absolute reflectance spectra were obtained by measuring the signal reflected in the THz divided by the signal of the gold evaporated sample. Broad-band room-temperature measurements have been obtained at the SapienzaTerahertz Laboratory at Sapienza University of Rome, through a Vertex 70v FTIR broad-band interferometer, for frequencies between 50 and 5000 cm^{-1}, and a JASCO v-770 IR-UV spectrometer for the interval from 3000 to 20,000 cm^{-1}. Data obtained from these measurements were merged to obtain the single broad-band reflectance curves (Figure 1b).

ASSOCIATED CONTENT

Data Availability Statement

Raw data were generated at the Synchrotron SOLEIL large-scale facility. Derived data supporting the findings of this study are available from the corresponding author upon request.

Supporting Information

The following files are available free of charge: The Supporting Information is available free of charge at https://pubs.acs.org/doi/10.1021/acsaelm.3c00506.

DC resistance, substrate analysis, multilayer stacking model, and superconducting gap determination (PDF)

AUTHOR INFORMATION

Corresponding Authors

Pascale Roy − *Synchrotron SOLEIL, L'Orme des Merisiers, 91192 Gif-sur-Yvette, France;* orcid.org/0000-0002-6350-4041; Email: pascale.roy@synchrotron-soleil.fr

Stefano Lupi − *Department of Physics, Sapienza University, 00185 Rome, Italy; INFN Section of Rome, 00185 Rome, Italy;* orcid.org/0000-0001-7002-337X; Email: stefano.lupi@uniroma1.it

Authors

Rebecca Cervasio − *Synchrotron SOLEIL, L'Orme des Merisiers, 91192 Gif-sur-Yvette, France*

Luca Tomarchio − *Department of Physics, Sapienza University, 00185 Rome, Italy; INFN Section of Rome, 00185 Rome, Italy;* orcid.org/0000-0003-0046-019X

Marine Verseils − *Synchrotron SOLEIL, L'Orme des Merisiers, 91192 Gif-sur-Yvette, France*

Jean-Blaise Brubach − *Synchrotron SOLEIL, L'Orme des Merisiers, 91192 Gif-sur-Yvette, France*

Salvatore Macis − *Department of Physics, Sapienza University, 00185 Rome, Italy; INFN—Laboratori Nazionali di Frascati, 00044 Frascati (Rome), Italy*

Shengwei Zeng − *Department of Physics, Faculty of Science, National University of Singapore, Singapore 117551, Singapore*

Ariando Ariando − *Department of Physics, Faculty of Science, National University of Singapore, Singapore 117551, Singapore;* orcid.org/0000-0002-0598-426X

Complete contact information is available at: https://pubs.acs.org/10.1021/acsaelm.3c00506

Author Contributions

The project was conceptualized and supervised by S.L. and P.R. Samples were synthesized and characterized by A.A. and

https://doi.org/10.1021/acsaelm.3c00506
ACS Appl. Electron. Mater. 2023, 5, 4770−4777

S.Z. Infrared measurements were carried out by L.T., R.C., M.V., J.B.B., S.M., and P.R. The data treatment was performed by L.T. and R.C. All authors contributed to the writing of the paper.

Funding

The project was funded through the PNRR MUR project PE0000023-NQSTI.

Notes

The authors declare no competing financial interest.

Code written for this study is available from the corresponding author upon request.

■ ACKNOWLEDGMENTS

A.A. acknowledges the discussion with L. E. Chow and S. K. Sudheesh and the financial support by the Ministry of Education MOE, Singapore, under its Tier-2 Academic Research Fund (AcRF), grant no. MOE-T2EP50121-0018. The authors also thank SOLEIL Synchrotron for providing synchrotron radiation through project number 20210595. They are thankful to A. Perrucchi and A. F. Santander-Syro for the guidance in the data treatment and to L. Manceron and K. Rader for the technical support. R.C. acknowledge financial support from the ED2MIB and the CPPS.

■ REFERENCES

(1) Bednorz, J. G.; Mueller, K. A. Possible high T_c superconductivity in the Ba-La-Cu-O system. *Z. Phys. B: Condens. Matter* **1986**, *64*, 189−193.

(2) Chaloupka, J.; Khaliullin, G. Orbital order and possible superconductivity in $LaNiO_3/LaMO_3$ superlattices. *Phys. Rev. Lett.* **2008**, *100*, 016404.

(3) Zhang, J.; Botana, A. S.; Freeland, J. W.; Phelan, D.; Zheng, H.; Pardo, V.; Norman, M. R.; Mitchell, J. F. Large orbital polarization in a metallic square-planar nickelate. *Nat. Phys.* **2017**, *13*, 864−869.

(4) Anisimov, V. I.; Bukhvalov, D.; Rice, T. M. Electronic structure of possible nickelate analogs to the cuprates. *Phys. Rev. B* **1999**, *59*, 7901−7906.

(5) Hayward, M. A.; Rosseinsky, M. J. Synthesis of the infinite layer Ni(I) phase $NdNiO_{2+x}$ by low temperature reduction of $NdNiO_3$ with sodiumhydride. *Solid State Sci.* **2003**, *5*, 839−850.

(6) Li, D.; Lee, K.; Wang, B.-Y.; Osada, M.; Crossley, S.; Lee, H. R.; Cui, Y.; Hikita, Y.; Hwang, H. Y. Superconductivity in an infinite-layer nickelate. *Nature* **2019**, *572*, 624−627.

(7) Zeng, S.; Tang, C. S.; Yin, X.; Li, C.; Li, M.; Huang, Z.; Hu, J.; Liu, W.; Omar, G. J.; Jani, H.; Lim, Z. S.; Han, K.; Wan, D.; Yang, P.; Pennycook, S. J.; Wee, A. T.-S.; Ariando, A. Phase diagram and superconducting dome of infinite-layer $Nd_{1-x}Sr_x$ NiO_2 thin films. *Phys. Rev. Lett.* **2020**, *125*, No. 147003.

(8) Hu, L.-H.; Wu, C. Two-band model for magnetism and superconductivity in nickelates. *Phys. Rev. Res.* **2019**, *1*, 032046.

(9) Liu, Z.; Ren, Z.; Zhu, W.; Wang, Z.; Yang, J. Electronic and magnetic structure of infinite-layer $NdNiO_2$: trace of antiferromagnetic metal. *npj Quantum Mater.* **2020**, *5*, No. 31.

(10) Kitatani, M.; Si, L.; Janson, O.; Arita, R.; Zhong, Z.; Held, K. Nickelate superconductors—a renaissance of the one-band Hubbard model. *npj Quantum Mater.* **2020**, *5*, No. 59.

(11) Lechermann, F. Late transition metal oxides with infinite-layer structure: nickelates versus cuprates. *Phys. Rev. B* **2020**, *101*, 081110.

(12) Werner, P.; Hoshino, S. Nickelate superconductors: multiorbital nature and spin freezing. *Phys. Rev. B* **2020**, *101*, 041104.

(13) Nomura, Y.; Hirayama, M.; Tadano, T.; Yoshimoto, Y.; Nakamura, K.; Arita, R. Formation of a two-dimensional single-component correlated electron system and band engineering in the nickelate superconductor $NdNiO_2$. *Phys. Rev. B* **2019**, *100*, 205138.

(14) Choi, M.-Y.; Lee, K.-W.; Pickett, W. E. Role of 4f states in infinite-layer $NdNiO_2$. *Phys. Rev. B* **2020**, *101*, 020503.

(15) Chen, H.; Hampel, A.; Karp, J.; Lechermann, F.; Millis, A. J. Mean Field Studies of Infinite Layer Nickelates: Physics Results and Methodological Implications. *Front. Phys.* **2022**, *10*, No. 835942.

(16) Zhou, T.; Gao, Y.; Wang, Z. Spin excitations in nickelate superconductors. *Sci. China Phys. Mech. Astron.* **2020**, *63*, No. 287412.

(17) Giaever, I. Energy Gap in Superconductors measured by electron tunneling. *Phys. Rev. Lett.* **1960**, *5*, 147−148.

(18) Dressel, M.; Wu, D.; BariŠić, N.; Gorshunov, B. Looking at the superconducting gap of iron pnictides. *J. Phys. Chem. Solids* **2011**, *72*, 514−518.

(19) Degiorgi, L.; Briceno, G.; Fuhrer, M. S.; Zettl, A.; Wachter, P. Optical measurements of the superconducting gap in single-crystal K_3C_{60} and Rb_3C_{60}. *Nature* **1994**, *369*, 541−543.

(20) Morse, R. W. *Progress in Cryogenics*; Heywood and Cy Ltd.: London, 1959; Vol. *I*, p 220.

(21) Phillips, N. E. Heat capacity of Aluminum between 0.1ŕK and 4.0ŕK. *Phys. Rev.* **1959**, *114*, 676−685.

(22) Warren, W. W.; Walstedt, R. E.; Brennert, G. F.; Espinosa, G. P.; Remeika, J. P. Evidence for two pairing energies from nuclear spin-lattice relaxation in superconducting $Ba_2YCu_3O_{7-\delta}$. *Phys. Rev. Lett.* **1987**, *59*, 1860−1863.

(23) Chow, L. E.; Kunniniyil Sudheesh, S.; Luo, Z. Y.; Nandi, P.; Heil, T.; Deuschle, J.; Zeng, S. W.; Zhang, Z. T.; Prakash, S.; Du, X. M.; Lim, Z. S.; van Aken, P. A.; Chia, E. E. M.; Ariando, A. Pairing symmetry in infinite-layer nickelate superconductorar. 2022, arXiv:2201.10038. arXiv.org e-Print archive. https://arxiv.org/abs/2201.10038.

(24) Harvey, S. P.; Wang, B. Y.; Fowlie, J.; Osada, M.; Lee, K.; Lee, Y.; Li, D.; Hwang, H. Y. Evidence for nodal superconductivity in infinite-layer nickelatesarxiv. 2022, arXiv:2201.12971. arXiv.org e-Print archive. https://arxiv.org/abs/2201.12971.

(25) Gu, Q.; Li, Y.; Wan, S.; Li, H.; Guo, W.; Yang, H.; Li, Q.; Zhu, X.; Pan, X.; Nie, Y.; Wen, H.-H. Single particle tunneling spectrum of superconducting $Nd_{1-x}Sr_xNiO_2$ thin films. *Nat. Commun.* **2020**, *11*, No. 6027.

(26) Dressel, M.; Drichko, N. Optical properties of two-dimensional organic conductors: signatures of charge ordering and correlation effects. *Chem. Rev.* **2004**, *104*, 5689−5716.

(27) Basov, D. N.; Timusk, T. Electrodynamics of high-T_c superconductors. *Rev. Mod. Phys.* **2005**, *77*, 721−779.

(28) Dressel, M.; Drichko, N.; Gorshunov, B.; Pimenov, A. THz spectroscopy of superconductors. *IEEE J. Sel. Top. Quantum Electron.* **2008**, *14*, 399−406.

(29) Perucchi, A.; Nicoletti, D.; Ortolani, M.; Marini, C.; Sopracase, R.; Lupi, S.; Schade, U.; Putti, M.; Pallecchi, I.; Tarantini, C.; Ferretti, M.; Ferdeghini, C.; Monni, M.; Bernardini, F.; Massidda, S.; Dore, P. Multiband conductivity and a multigap superconducting phase in films from optical measurements at terahertz frequencies. *Phys. Rev. B* **2010**, *81*, No. 092509.

(30) Tinkham, M. *Introduction to Superconductivity*; Mc Graw-Hill: New York,, 1996.

(31) Timusk, T.; Tanner, D. *Physical Properties of High Temperature Superconductors I*; World Scientific: Singapore, 1989.

(32) Timusk, T.; Tanner, D. *Physical Properties of High Temperature Superconductors III*; World Scientific: Singapore, 1992.

(33) Peng, W.-w.; Tétot, R.; Niu, G.; Amzallag, E.; Vilquin, B.; Brubach, J.-B.; Roy, P. Room-temperature soft mode and ferroelectric like polarization in $SrTiO_3$ ultrathin films: Infrared and ab initio study. *Sci. Rep* **2017**, *7*, No. 2160, DOI: 10.1038/s41598-017-02113-4.

(34) Petzelt, J.; Ostapchuk, T.; Gregora, I.; Rychetský, I.; Hoffmann-Eifert, S.; Pronin, A. V.; Yuzyuk, Y.; Gorshunov, B. P.; Kamba, S.; Bovtun, V.; Pokorný, J.; Savinov, M.; Porokhonskyy, V.; Rafaja, D.; Vaněk, P.; Almeida, A.; Chaves, M. R.; Volkov, A. A.; Dressel, M.; Waser, R. Dielectric, infrared, and Raman response of undoped $SrTiO_3$ ceramics: Evidence of polar grain boundaries. *Phys. Rev. B* **2001**, *64*, No. 184111.

(35) Kuzmenko, A. B. Kramers-Kronig constrained variational analysis of optical spectra. *Rev. Sci. Instrum.* **2005**, *76*, No. 083108.

(36) Heavens, O. S.; Singer, S. F. Optical properties of thin solid films. *Phys. Today* **1956**, *9*, 24−26.
(37) Heavens, O. S. *Thin Film Physics*; Methuen and Co. LTDA: London,, 1970.
(38) Homes, C. C.; Lobo, R. P. S. M.; Fournier, P.; Zimmers, A.; Greene, R. L. Optical determination of the superconducting energy gap in electron-doped $Pr_{1.85}Ce_{0.15}CuO_4$. *Phys. Rev. B* **2006**, *74*, No. 214515, DOI: 10.1103/PhysRevB.74.214515.
(39) Puchkov, A. V.; Fournier, P.; Basov, D. N.; Timusk, T.; Kapitulnik, A.; Kolesnikov, N. N. Evolution of the pseudogap state of high- T_c superconductors with doping. *Phys. Rev. Lett.* **1996**, *77*, 3212−3215.
(40) Tu, J. J.; Homes, C. C.; Gu, G. D.; Basov, D. N.; Strongin, M. Optical studies of charge dynamics in optimally doped $Bi_2Sr_2CaCu_2O_{8+}$. *Phys. Rev. B* **2002**, *66*, No. 144514.
(41) Lucarelli, A.; Lupi, S.; Ortolani, M.; Calvani, P.; Maselli, P.; Capizzi, M.; Giura, P.; Eisaki, H.; Kikugawa, N.; Fujita, T.; Fujita, M.; Yamada, K. Phase diagram of $La_{2x}Sr_xCuO_4$ probed in the infared: imprints of charge stripe excitations. *Phys. Rev. Lett.* **2003**, *90*, No. 037002.
(42) Lupi, S.; Maselli, P.; Capizzi, M.; Calvani, P.; Giura, P.; Roy, P. Evolution of a polaron band through the phase diagram of $Nd_{2x}Ce_xCuO_{4-y}$. *Phys. Rev. Lett.* **1999**, *83*, 4852−4855.
(43) Congeduti, A.; Postorino, P.; Dore, P.; Nucara, A.; Lupi, S.; Mercone, S.; Calvani, P.; Kumar, A.; Sarma, D. D. Infrared study of charge delocalization induced by pressure in the $La_{0.75}Ca_{0.25}MnO_3$ Manganite. *Phys. Rev. B* **2001**, *63*, No. 184410.
(44) Lupi, S.; Ortolani, M.; Calvani, P. Optical conductivity of single crystals of $Na_{0.57}CoO_2$. *Phys. Rev. B* **2004**, *69*, No. 180506.
(45) Lo Vecchio, I.; Baldassarre, L.; D'Apuzzo, F.; Limaj, O.; Nicoletti, D.; Perucchi, A.; Fan, L.; Metcalf, P.; Marsi, M.; Lupi, S. Optical properties of V_2O_3 in its whole phase diagram. *Phys. Rev. B* **2015**, *91*, 155133.
(46) Degiorgi, L. Electronic correlations in iron-pnictide superconductors and beyond: lessons learned from optics. *New J. Phys.* **2011**, *13*, 023011.
(47) Chow, L. E.; Ariando, A. A. Infinite-Layer Nickelate Superconductors: A Current Experimental Perspective of the Crystal and Electronic Structures. *Front. Phys.* **2022**, *10*, No. 834658, DOI: 10.3389/fphy.2022.834658.
(48) Yu, Y.; Ma, L.; Cai, P.; Zhong, R.; Ye, C.; Shen, J.; Gu, G. D.; Chen, X. H.; Zhang, Y. High-temperature superconductivity in monolayer $Bi_2Sr_2CaCu_2O_{8+\delta}$. *Nature* **2019**, *575*, 156−163.
(49) Homes, C. C.; Dordevic, S. V.; Strongin, M.; Bonn, D. A.; Liang, R.; Hardy, W. N.; Komiya, S.; Ando, Y.; Yu, G.; Kaneko, N.; Zhao, X.; Greven, M.; Basov, D. N.; Timusk, T. A universal scaling relation in high-temperature superconductors. *Nature* **2004**, *430*, 539−541.
(50) Homes, C. C.; Dordevic, S. V.; Valla, T.; Strongin, M. Scaling of the superfluid density in high-temperature superconductors. *Phys. Rev. B* **2005**, *72*, No. 134517.
(51) Tallon, J. L.; Cooper, J. R.; Naqib, S. H.; Loram, J. W. Scaling relation for the superfluid density of cuprate superconductors: Origins and limits. *Phys. Rev. B* **2006**, *73*, No. 180504.
(52) Mattis, D. C.; Bardeen, J. Theory of the anomalous skin effect in normal and superconducting metals. *Phys. Rev.* **1958**, *111*, 412−417.
(53) Talantsev, E. F. Classifying superconductivity in an infinite-layer nickelate Nd0.8Sr0.2NiO2. *Results Phys.* **2020**, *17*, No. 103118.
(54) Li, Z.; Louie, S. G. Two-gap superconductivity and decisive role of rare-earth d electrons in infinite-layer nickelates. 2022, arXiv:2210.12819. arXiv.org e-Print archive. https://arxiv.org/abs/2210.12819.
(55) Rugheimer, N. M.; Lehoczky, A.; Briscoe, C. V. Microwave transmission- and reflection-coefficient ratios of thin superconducting films. *Phys. Rev.* **1967**, *154*, 414.
(56) Palmer, L. H.; Tinkham, M. Far-infrared absorption in thin superconducting Lead films. *Phys. Rev.* **1968**, *165*, 588.
(57) Seibold, G.; Benfatto, L.; Castellani, C. Application of the Mattis-Bardeen theory in strongly disordered superconductors. *Phys. Rev. B* **2017**, *96*, No. 144507, DOI: 10.1103/PhysRevB.96.144507.
(58) Gross, F.; Chandrasekhar, B. S.; Einzel, D.; Andres, K.; Hirschfeld, P. J.; Ott, H. R.; Beuers, J.; Fisk, Z.; Smith, J. L. Anomalous temperature dependence of the magnetic field penetration depth in superconducting uranium-beryllium (UBe_{13}). *Z. Phys. B: Condens. Matter* **1986**, *64*, 175−188.
(59) Prozorov, R.; Giannetta, R. W. Magnetic penetration depth in unconventional superconductors. *Supercond. Sci. Technol.* **2006**, *19*, R41−R67.
(60) Roy, P.; Rouziéres, M.; Qi, Z.; Chubar, O. The AILES Infrared Beamline on the third generation synchrotron radiation facility SOLEIL. *Infrared Phys. Technol.* **2006**, *49*, 139−146.

https://doi.org/10.1021/acsaelm.3c00506
ACS Appl. Electron. Mater. 2023, 5, 4770−4777